Mineralogical Magazine, October 2013, Vol. 77(7), pp. 3027–3037

Oxycalcioroméite, $Ca_2Sb_2O_6O$, from Buca della Vena mine, Apuan Alps, Tuscany, Italy: a new member of the pyrochlore supergroup

C. Biagioni[1,*], P. Orlandi[1], F. Nestola[2] and S. Bianchin[3]

[1] Dipartimento di Scienze della Terra, Università di Pisa, Via S. Maria 53, I-56126 Pisa, Italy
[2] Dipartimento di Geoscienze, Università di Padova, Via Gradenigo 6, I-35131 Padova, Italy
[3] ICIS-CNR, Corso Stati Uniti 4, I-35127 Padova, Italy

[*Received 22 May 2013; Accepted 19 September 2013; Associate Editor: S. Krivovichev*]

ABSTRACT

The new mineral species oxycalcioroméite, $Ca_2Sb_2^{5+}O_6O$, has been discovered at the Buca della Vena mine, Stazzema, Apuan Alps, Tuscany, Italy. It occurs as euhedral octahedra, up to 0.1 mm in size, embedded in dolostone lenses in the baryte + pyrite + iron oxides ore. Associated minerals are calcite, cinnabar, derbylite, dolomite, hematite, 'mica', pyrite, sphalerite and 'tourmaline'. Oxycalcioroméite is reddish-brown in colour and transparent. It is isotropic, with n_{calc} = 1.950.

Electron microprobe analysis gave (wt.%; n = 6) Sb_2O_5 63.73, TiO_2 3.53, SnO_2 0.28, Sb_2O_3 10.93, V_2O_3 0.68, Al_2O_3 0.28, PbO 0.68, FeO 5.52, MnO 0.13, CaO 13.68, Na_2O 0.83, F 1.20, O = F − 0.51, total 100.96. No H_2O, above the detection limit, was indicated by either infrared or micro-Raman spectroscopies. The empirical formula, based on 2 cations at the B site, is $(Ca_{1.073}Fe^{2+}_{0.338}Sb^{3+}_{0.330}Na_{0.118}Pb_{0.013}Mn_{0.008})_{\Sigma=1.880}(Sb^{5+}_{1.734}Ti_{0.194}V_{0.040}Al_{0.024}Sn_{0.008})_{\Sigma=2.000}(O_{6.682}F_{0.278})_{\Sigma6.960}$. The crystal structure study gives a cubic unit cell, space group $Fd\bar{3}m$, with a 10.3042(7) Å, V 1094.06(13) Å^3, Z = 8. The five strongest X-ray powder diffraction lines are [d (Å)I (visually estimated)(hkl)]: 3.105(m)(311); 2.977(s)(222); 2.576(m)(400); 1.824(ms)(440); and 1.556(ms)(622). The crystal structure of oxycalcioroméite has been solved by X-ray single-crystal study on the basis of 114 observed reflections, with a final R_1 = 0.0114. It agrees with the general features of the members of the pyrochlore supergroup.

Keywords: oxycalcioroméite, new mineral species, pyrochlore supergroup, roméite group, Buca della Vena mine, Apuan Alps, Tuscany, Italy, crystal structure.

Introduction

The nomenclature of the minerals belonging to the pyrochlore supergroup was revised by Atencio *et al*. (2010) and is based on the ions at the *A*, *B* and *Y* sites. Five groups have been defined, on the basis of the dominant cation at the *B* site: pyrochlore (Nb), microlite (Ta), roméite (Sb), betafite (Ti), and elsmoreite (W) groups. This new nomenclature uses names composed of two prefixes and one root name, identical to the group name. The first prefix refers to the dominant ion (usually an anion) of the dominant valence at the *Y* site, whereas the second prefix refers to the dominant cation of the dominant valence at the *A* site. When the new nomenclature scheme was approved (Atencio *et al*., 2010), only seven names referred to valid species, whereas for another twenty names a complete description and definition of the type specimens was needed. Recently, other mineral species have been added to the pyrochlore supergroup (Table 1).

* E-mail: biagioni@dst.unipi.it
DOI: 10.1180/minmag.2013.077.7.12

TABLE 1. Approved mineral species in the pyrochlore supergroup.

Mineral name	Chemical formula	Ref.
Fluorcalciomicrolite	$(Ca,Na)_2Ta_2(O,OH)_6F$	Andrade *et al*. (2012)
Fluorcalcioroméite	$(Ca,Na)_2Sb_2^{5+}(O,OH)_6F$	Atencio *et al*. (2013)
Fluornatromicrolite	$(Na_{1.5}Bi_{0.5})Ta_2O_6F$	Witzke *et al*. (2011)
Hydrokenoelsmoreite	$\square_2W_2O_6(H_2O)$	Atencio *et al*. (2010)
Hydrokenomicrolite	$(\square,H_2O)_2Ta_2(O,OH)_6(H_2O)$	Andrade *et al*. (2013)
Hydropyrochlore	$(H_2O,\square)_2Nb_2(O,OH)_6(H_2O)$	Atencio *et al*. (2010)
Hydroxycalciopyrochlore	$(Ca,Na,U,\square)_2(Nb,Ti)_2O_6(OH)$	Atencio *et al*. (2010)
Hydroxycalcioroméite	$(Ca,Sb^{3+})_2(Sb^{5+},Ti)_2O_6(OH)$	Atencio *et al*. (2010)
Hydroxykenomicrolite	$(\square,Na,Sb^{3+})_2Ta_2O_6(OH)$	Atencio *et al*. (2010)
Hydroxymanganopyrochlore	$(Mn,Th,Na,Ca,\textit{REE})_2(Nb,Ti)_2O_6(OH)$	Chukanov *et al*. (2013)
Oxycalciopyrochlore	$Ca_2Nb_2O_6O$	Atencio *et al*. (2010)
Oxycalcioroméite	$Ca_2Sb_2O_6O$	This work
Oxystannomicrolite	$Sn_2Ta_2O_6O$	Atencio *et al*. (2010)
Oxystibiomicrolite	$(Sb^{3+},Ca)_2Ta_2O_6O$	Atencio *et al*. (2010)

During a study of the mineral assemblage at the Buca della Vena mine, Apuan Alps, Tuscany, Italy, a member of the pyrochlore supergroup was identified. Initially, the mineral was reported as 'stibiobetafite' (Orlandi and Dini, 2004) on the basis of a qualitative chemical analysis. "Stibiobetafite" was defined by Černý *et al*. (1979) as the Sb^{3+} analogue of betafite; according to the new nomenclature it is correctly classified as oxycalciopyrochlore (Atencio *et al*., 2010). A quantitative chemical analysis of the phase from Buca della Vena mine showed that Ti cannot be the dominant cation at the *B* site, owing to its small content (~3.5 wt.%), whereas Sb is abundant. Consequently, the phase belongs to the roméite group. Chemical, spectroscopic and structural data point to the absence of H_2O and a very limited amount of fluorine, indicating an 'oxy' composition at the *Y* site; at the *A* site, the dominant cation of the dominant valence is calcium. Consequently, in agreement with Atencio *et al*. (2010), the mineral has to be named 'oxycalcioroméite'. A mineral corresponding to oxycalcioroméite was characterized chemically by Christy and Gatedal (2005) from Långban, Värmland, Sweden, but crystallographic data are missing.

The new finding from the Buca della Vena mine allowed us to propose the approval of oxycalcioroméite as a valid mineral species. The mineral and its name were approved by the IMA-CNMNC, under the number 2012-022. The holotype specimen of oxycalcioroméite is deposited in the mineralogical collection of the Museo di Storia Naturale, Università di Pisa, Via Roma 79, Calci, Pisa, Italy, with catalogue number 19640. As stated above, the name is in agreement with the nomenclature of the pyrochlore supergroup (Atencio *et al*., 2010; Christy and Atencio, 2013).

Geological setting and occurrence

The Buca della Vena mine (latitude 43º59'N, longitude 10º18'E) exploited a small baryte + pyrite + iron oxides ore deposit embedded at the contact between a metavolcanic-metasedimentary sequence of Palaeozoic–Triassic age (Scisti di Fornovolasco formation) and Upper Triassic dolostone and Lower Jurassic Marbles. The geological setting of the Buca della Vena mine has been described by previous authors (Carmignani *et al*., 1976; Cortecci *et al*., 1985; Orberger, 1985; Benvenuti *et al*., 1986); the orebody is represented by a lens-shaped body, 200 m long and 1 to 20 m thick, having a NNE−SSW direction and dipping 15−30º SE.

The ore body is zoned, with baryte + pyrite at the bottom and baryte + iron oxides (magnetite and hematite) at the top; lenses of marbles and dolostones are intercalated in the ore. During the Alpine tectono-metamorphic events, these carbonatic lenses were deformed and fractured, with the formation of calcite + baryte vein systems hosting rare minerals, among which nine mineral species have Buca della Vena as type locality (see Biagioni, 2009, for a review).

Oxycalcioroméite was identified in specimens collected in the southern part of the mine, in association with calcite, cinnabar, derbylite, dolomite, hematite, 'mica', pyrite, sphalerite and 'tourmaline'. Its crystallization is related to the circulation of hydrothermal fluids during the Alpine metamorphism (*P-T* conditions belonging to the greenschist facies; Fellin *et al*., 2007 and references therein) of the baryte + pyrite + iron oxides ore deposit of Buca della Vena mine.

Mineral description

Oxycalcioroméite occurs as transparent {111} crystals (Fig. 1), up to 0.1 mm long, reddish-brown in colour, with a pale-yellow streak and a vitreous to resinous lustre. It does not fluoresce under UV light. Oxycalcioroméite is brittle, with an irregular fracture. Its hardness and density were not measured, owing to the scarcity of available material and its small size; the calculated density, based on the empirical formula, is 5.393 g cm^{-3}.

Oxycalcioroméite is isotropic, with a reddish-brown colour in thin section; refractive index was higher than those of the available liquids. The refractive index was calculated using the Gladstone-Dale relation (Mandarino, 1979, 1981); assuming the empirical formula, the n_{calc} is 1.950.

Chemical data

Preliminary qualitative chemical analyses were performed using a Philips XL-30 scanning electron microscope equipped with an EDAX DX4 system operating in energy-dispersive mode. The only elements with $Z > 8$ detected in the studied samples are Sb, Ca, Fe, Ti, Na and minor F.

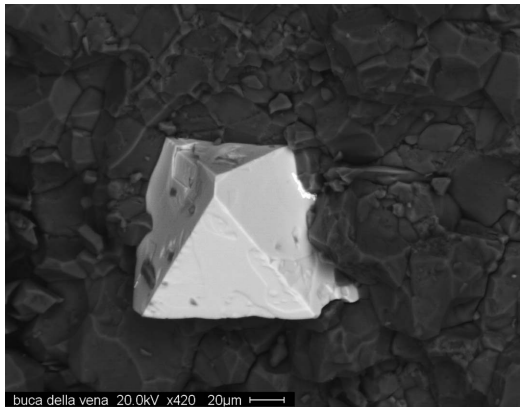

FIG. 1. Oxycalcioroméite, {111} crystal with anhedral crystals of dolomite.

Electron-microprobe analysis was carried out using a Cameca SX50 at the Electron-microprobe laboratory of the CNR-Institute for Geosciences and Earth Resources of Padova, Italy, under the following analytical conditions: accelerating voltage 20 kV, beam current 20 nA, beam size 1−2 µm. The counting time for one spot analysis was 10 s per peak. Standards (element, emission line) are: apatite (F*K*α), albite (Na*K*α), diopside (Si*K*α, Ca*K*α), Al_2O_3 (Al*K*α), vanadinite (V*K*α), $MnTiO_3$ (Ti*K*α, Mn*K*α), Fe_2O_3 (Fe*K*α), SnO_2 (Sn*L*α), Sb_2S_3 (Sb*L*α) and PbS (Pb*M*α). Mg, Si, K, Cr, Sr, Nb, Ce and U were sought but found to be below the detection limit.

Chemical data are reported in Table 2; the Sb_2O_5:Sb_2O_3 ratio was calculated in agreement with crystal-chemical considerations (see Crystal chemistry section). The chemical formula, based on 2 cations at the *B* site, in agreement with Atencio *et al*. (2010), is $(Ca_{1.073}Fe^{2+}_{0.338}Sb^{3+}_{0.330}Na_{0.118}Pb^{2+}_{0.013}Mn^{2+}_{0.008})_{\Sigma=1.880}(Sb^{5+}_{1.734}Ti_{0.194}V^{3+}_{0.040}Al_{0.024}Sn^{4+}_{0.008})_{\Sigma=2.000}(O_{6.682}F_{0.278})_{\Sigma 6.960}$.

The simplified formula of oxycalcioroméite is $Ca_2Sb^{5+}_2O_7$, which requires (in wt.%) CaO 25.74, Sb_2O_5 74.26, total 100.00.

Infrared and micro-Raman spectroscopy

Micro-FTIR analyses were performed using a Continµum Nicolet microscope connected to a Thermofisher iS-10 system and equipped with a Mercury Cadmium Telluride (MCT) detector used for spectra collection. The infrared (IR) spectra were collected in reflectance mode in the range 650−4000 cm^{-1}, with a resolution of 4 cm^{-1}. The oxycalcioroméite spectrum is shown in Fig. 2. The significant spectrum background is probably due to the small size of the crystal analysed.

With respect to the infrared spectrum of hydroxycalcioroméite (formerly indicated as "lewisite", see Atencio *et al*., 2010) reported by Rouse *et al*. (1998) and showing a sharp peak at ~3590 cm^{-1} and a small shoulder at ~3560 cm^{-1}, our specimen did not show any peak in the O−H bending and stretching regions. A similar sharp absorption peak at 3613 cm^{-1} was observed by Brugger *et al*. (1997) in a roméite-group mineral from Praborna, Italy; on the contrary, the specimen from Fianel, Switzerland, showed no such peak, owing to its F-rich nature, with fluorine completely filling the *Y* site (recently

TABLE 2. Electron-microprobe analysis of oxycalcioroméite.

	Wt.%	Range	e.s.d.
$Sb_2O_5^{tot}$	75.86	75.23–76.25	0.40
Sb_2O_5	63.73		
Sb_2O_3	10.93		
TiO_2	3.53	2.18–4.33	0.92
SnO_2	0.28	0.19–0.37	0.06
V_2O_3	0.68	0.59–0.85	0.10
Al_2O_3	0.28	0.26–0.31	0.02
CaO	13.68	13.34–13.82	0.17
MnO	0.13	0.11–0.14	0.01
FeO	5.52	5.32–5.86	0.20
PbO	0.68	0.60–0.76	0.06
Na_2O	0.83	0.78–1.03	0.10
F	1.20	0.67–1.59	0.34
Sub-total	101.47		
O = F	–0.51		
Total	100.96		

e.s.d.: estimated standard deviation

samples from Fianel have been used for the definition of fluorcalcioroméite; Atencio *et al*., 2013). As shown by electron-microprobe analyses, our specimen is F-poor and, being virtually devoid of OH, its *Y* site has to be occupied preferentially by an oxygen atom.

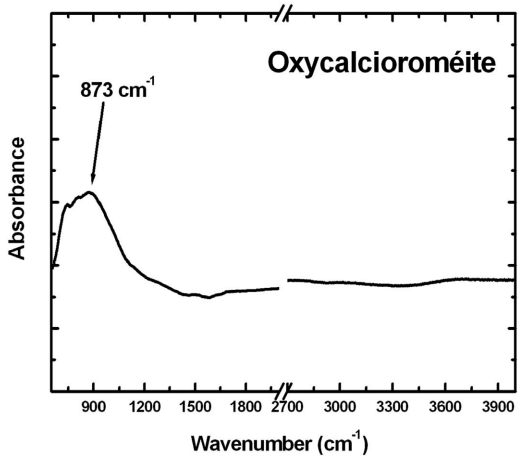

FIG. 2. IR spectrum of oxycalcioroméite collected on a single crystal between 650 and 4000 cm^{-1}. The spectrum was divided into two parts: the first between 650 and 2000 cm^{-1}, the second between 2700 and 4000 cm^{-1}, in order to include both the H_2O bending region and the OH-stretching region.

Micro-Raman spectra were collected using a Thermo Scientific DXR Raman Microscope, using a 532 nm laser, 50× objective, with a spectral resolution of 2 cm^{-1} and a spot size of ~2 μm. The main feature of the observed spectrum (Fig. 3) is the strong band at 509 cm^{-1}, in agreement with the spectra of other members of the roméite group studied by Bahfenne and Frost (2009, 2010) and Frost and Bahfenne (2010). As pointed out by those authors, very few studies have been published on the spectroscopy of antimonate minerals and the correct attribution of the Raman as well as the infrared bands should be considered only speculative. We can hypothesize that the band at 873 cm^{-1} and those in the range 200 to 950 cm^{-1} in the infrared and micro-Raman spectra, respectively, could be assigned to Sb–O vibrations, in agreement with Frost and Bahfenne (2010) and Bahfenne and Frost (2009, 2010). Following these authors, we propose that the strong micro-Raman bands at 509 and 666 cm^{-1} could be assigned to the stretching of Sb–O bonds, probably as well as the band at 777 cm^{-1}. The low-intensity bands at 295 and 199 cm^{-1} could be interpreted as due to O–Sb–O bending and to lattice vibrations, respectively. The interpretation of the remaining bands is difficult. Micro-Raman spectroscopy did not reveal the presence of bands in the spectral range characterized by O–H bending and stretching vibrations, confirming the

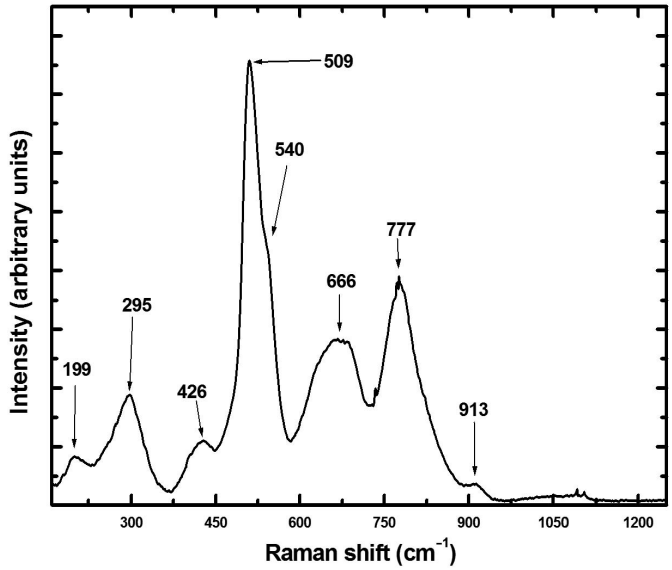

FIG. 3. Micro-Raman spectrum of oxycalcioroméite.

virtually anhydrous character of the specimen studied, as already shown by the IR spectroscopy.

Crystallography

The X-ray powder diffraction (XRPD) pattern of oxycalcioroméite was obtained using a 114.6 mm-diameter Gandolfi camera, with Ni-filtered Cu$K\alpha$ radiation. The observed XRPD pattern was compared with the calculated one (obtained using the software *PowderCell*; Kraus and Nolze, 1996) in Table 3. The unit-cell parameters refined from the XRPD pattern using the *Unit Cell* software (Holland and Redfern, 1997) on the basis of 12 unequivocally indexed reflections are a 10.3102(7) Å, V 1096.0(1) Å^3.

Intensity data were collected using a crystal fragment (0.04 mm × 0.04 mm × 0.02 mm) mounted on a Bruker Smart Breeze diffractometer operating at 50 kV and 30 mA and equipped with an air-cooled CCD detector. Graphite monochromated Mo$K\alpha$ radiation was used. 531 frames were collected in 0.5º slices with an exposure time of 10 s per frame. The detector-to-crystal working distance was set at 50 mm. Data were integrated and corrected for Lorentz and polarization, background effects, and absorption using *Apex 2* (Bruker AXS Inc. 2004), resulting in 117 independent reflections. The structure was solved by direct methods using *Shelxs-97* and refined using *Shelx-97* (Sheldrick, 2008). The space group symmetry was $Fd\bar{3}m$; no violations of the d glide were observed. Site-scattering values were refined

TABLE 3. Observed and calculated X-ray powder diffraction data for oxycalcioroméite.

I_{obs}	d_{meas}	I_{calc}	d_{calc}	h k l
mw	5.93	32	5.949	1 1 1
m	3.105	24	3.107	3 1 1
s	2.977	100	2.976	2 2 2
m	2.576	24	2.576	4 0 0
vw	2.363	1	2.364	3 3 1
w	2.103	1	2.103	4 2 2
m	1.984	2	1.983	5 1 1
		6	1.983	3 3 3
vs	1.824	45	1.821	4 4 0
m	1.744	6	1.742	5 3 1
vw	1.628	1	1.629	6 2 0
mw	1.572	4	1.571	5 3 3
vs	1.556	34	1.553	6 2 2
m	1.489	8	1.487	4 4 4
m	1.446	4	1.443	5 5 1
		1	1.443	7 1 1

The d_{hkl} values were calculated on the basis of the unit cell refined by using single-crystal data. Intensities were calculated on the basis of the structural model. Observed intensities were visually estimated. vs = very strong; s = strong; m = medium; mw = medium-weak; w = weak; vw = very weak.

using neutral scattering curves taken from the *International Tables for X-ray Crystallography* (Wilson, 1992). Initially, the following curves were used: Ca *vs.* □ at the *A* site, Sb *vs.* □ at the *B* site, O *vs.* □ at the O and *Y* site. After several cycles of isotropic refinement, the R_1 converged to 0.038%; introducing the anisotropic displacement parameters for cations and anions, R_1 dropped to 0.018%. The mean site scattering values at the different sites suggested a full occupancy at the *A* site (~19.4 e^-), whereas Sb was substituted by lighter atom(s) at the *B* site (45.4 e^-). The O site was completely filled by an oxygen atom (7.7 e^-), whereas a small excess of electrons was observed at the *Y* site (~9 e^-). The difference-Fourier map showed the presence of a small maximum at the 96*g* position, suggesting a splitting of the *A* site. The maximum residual close to the *A* site was attributed to the splitting of this site owing to the different coordination environments of Ca^{2+} and Sb^{3+} cations; the 16*d* position hosts Ca^{2+}, whereas stereoactive cations (i.e. Sb^{3+}) are hosted in the less symmetrical position 96*g*, in agreement with Rouse *et al.* (1998). Due to their proximity (~0.5 Å), these two sub-positions cannot be occupied simultaneously. A new refinement was started refining Ca *vs.* Sb at the *A* and *A′* sub-positions, respectively, and Sb *vs.* Ti at the *B* site. The site occupancy of O (labelled as O1) was fixed at a full occupancy, whereas the site occupancy of *Y* (labelled as O2) was freely refined. The excess of electron density observed at the *Y* site could be interpreted as due to the presence of minor cations (e.g. Pb^{2+}) at this position, like in inverse pyrochlore (Ercit *et al.*, 1993).

After ten cycles of anisotropic least-square refinements, the final R_1 factor converged to 0.011% for 114 observed reflections and 18 parameters. The largest peak and hole in the final difference-Fourier map were 0.31 and −0.36 e $Å^{-3}$.

Details of the data collection and refinement are reported in Table 4.

Crystal-structure description

Atomic coordinates, displacement parameters, and selected bond distances are reported in Tables 5

TABLE 4. Crystal data and summary of parameters describing data collection and refinement for oxycalcioroméite.

Crystal data	
Crystal size (mm)	0.04 × 0.04 × 0.02
Cell setting, space group	Cubic, $Fd\bar{3}m$
a (Å)	10.3042(7)
V ($Å^3$)	1094.06(13)
Z	8
Data collection and refinement	
Radiation, wavelength (Å)	Mo*K*α, 0.71073
Temperature (K)	293
Maximum observed 2θ (º)	63.98
Measured reflections	969
Unique reflections	117
Reflections $F_o > 4\sigma(F_o)$	114
R_{int} after absorption correction	0.0106
$R\sigma$	0.0069
Range of *h*, *k*, *l*	$-15 \leqslant h \leqslant 15$, $-12 \leqslant k \leqslant 10$, $-12 \leqslant l \leqslant 10$
R [F_o>4σ (F_o)]	0.0114
R (all data)	0.0123
wR (on F_o^2)	0.0290
Goof	1.270
Number of least-squares parameters	18
Maximum and minum residual peak ($e/Å^3$)	0.31 (at 0.81 Å from O2) –0.36 (at 0.57 Å from Sb3)

TABLE 5. Atomic coordinates and displacement parameters (Å^2) for oxycalcioroméite. U_{eq} is defined as one third of the trace of the orthogonalized U^{ij} tensor.

Site	Wyckoff site	x	y	z	U^{11}	U^{22}	U^{33}	U^{12}	U^{13}	U^{23}	U_{eq}
A	16d	½	½	½	0.0214(7)	U^{11}	U^{11}	–0.0047(6)	U^{12}	U^{12}	0.0214(7)
A'	96g	0.482(2)	0.482(2)	0.544(2)	0.0214(7)	U^{11}	U^{11}	–0.0047(6)	U^{12}	U^{12}	0.0214(7)
B	16c	0	0	0	0.0053(2)	U^{11}	U^{11}	–0.0004(1)	U^{12}	U^{12}	0.0053(2)
O1	48f	0.3241(2)	⅛	⅛	0.0104(10)	0.0104(7)	U^{22}	0	U^{12}	0.0052(8)	0.0104(6)
O2	8b	⅜	⅜	⅜	0.0190(15)	U^{11}	U^{11}	0	0	0	0.0190(15)

TABLE 6. Selected interatomic distances (Å) in oxycalcioroméite.

A	–O2	2.2309(2) × 2
	–O1	2.570(2) × 6
	average	2.485
A'	–O1	2.07(4)
	–O2	2.24(3)
	–O2	2.34(3)
	–O1	2.35(1) × 2
	average	2.27
	–O1	2.87(2) × 2
	–O1	3.07(4)
B	–O1	1.975(1) × 6

and 6. The crystal structure of oxycalcioroméite (Fig. 4) is characterized by BO_6 octahedra polymerized to form the framework typical of the pyrochlore structure. The framework shows [110] tunnels hosting the A and Y sites.

Cations hosted at the A site are eight-fold coordinated; the $<A-\varphi>$ bond length, where φ is an anion hosted at the O and Y sites, is 2.485 Å, in agreement with hydroxycalcioroméite, 2.478 Å (Rouse *et al*., 1998). Hydroxycalcioroméite, studied by Rouse *et al*. (1998), was very enriched in Sb, with this cation occurring in two valence states, i.e. Sb^{3+} and Sb^{5+}. Whereas the latter is hosted at the B site, the former occurs at the A site. As stated above, Sb^{3+} is displaced from the 16d position to the less symmetrical 96g position, assuming a five-fold coordination. The $<Sb^{3+}-O>$ is 2.27 Å, in good agreement with the average bond-length in hydroxycalcioroméite, 2.277 Å (Rouse *et al*., 1998). The site population at the A site (including the split position A') is $(Ca_{0.536}Fe^{2+}_{0.169}Sb^{3+}_{0.165}Na_{0.059}Mn_{0.004})$; taking into account the site multiplicity, it corresponds to a calculated site scattering of 48.6 electrons per formula unit (e.p.f.u.), to be compared with the observed site scattering value of 44.4 e.p.f.u.

The B site has a regular six-fold coordination, with $B-O$ bond length of 1.975 Å; its site population is $(Sb^{5+}_{0.867}Ti_{0.097}Al_{0.012}V^{3+}_{0.020}Sn^{4+}_{0.004})$, corresponding to a calculated site scattering (taking into account the site multiplicity) of 95.8 e.p.f.u., to be compared with 94.4 e.p.f.u. obtained through the crystal-structure refinement. The uncertainties in the oxidation state of Sn (+2 or +4) influences its correct assignments at the A or B sites; in fact, Sn^{2+} has a larger ionic radius,

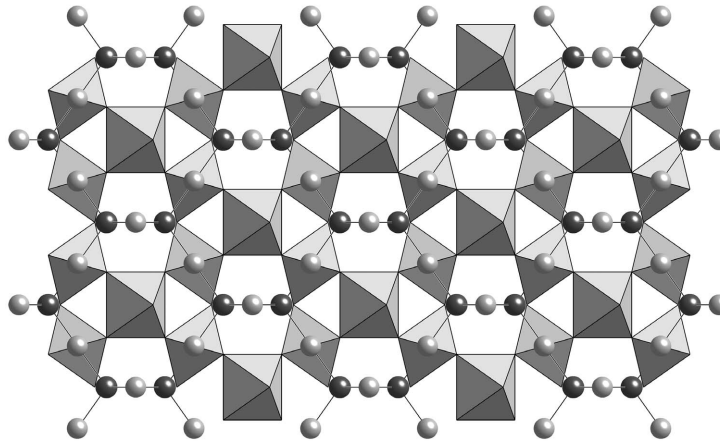

FIG. 4. Crystal structure of oxycalcioroméite as seen down [110], **c** horizontal. Polyhedra: *B* site. Circles: *A* site (light grey) and *Y* site (dark grey). The split *A′* site is not shown.

compatible with its occurrence at the *A* site, whereas Sn^{4+} prefers a six-fold coordination. Owing to the very small Sn content of the studied material, the occurrence of tin at the *A* or *B* site does not significantly affect the calculation of the site scattering value.

The excess of electron density at the *Y* site could be interpreted as related to the substitution of oxygen atoms by a cation, e.g. Pb^{2+}. It is known that in natural members of the pyrochlore supergroup, Pb is present at the divalent state and should occupy the *A* site or, by analogy with pyrochlore-type compounds incorporating large cations, at the *Y* site of the inverse pyrochlore structure (Bindi *et al*., 2006). Assuming a site population $[(O_{0.682}F_{0.278})Pb^{2+}_{0.013}]$ at the *Y* site, the calculated site scattering would be 9.0 e.p.f.u., to be compared with an observed value of 9.3 e.p.f.u.

Crystal chemistry

Owing to the complex crystal chemistry of the members of the roméite group and the possible different ion substitutions, some comments are needed to justify the cation distribution proposed in the 'Chemical data' section. This distribution is based not only on the electron-microprobe analysis and spectroscopic data, but also on the result of the crystallographic study, as shown by the comparison between calculated and observed site-scattering values. Some issues remain to be discussed: (1) iron oxidation state; (2) Sb^{5+}:Sb^{3+} ratio; and (3) Ca^{2+}–Na^{+} substitution.

Iron oxidation state

Taking into account the ionic radii of Fe^{2+} and Fe^{3+} in six- and eight-fold coordination (Shannon, 1976), it can be concluded that, in the crystal structure of pyrochlore-like phases, Fe^{2+} and Fe^{3+} ions may be preferentially hosted at the *A* and *B* sites, respectively.

In natural members of the roméite group there are some ambiguities with respect to the correct assignment of Fe. Usually, the iron concentration in these minerals is small (e.g. up to 0.09 Fe^{2+} a.p.f.u. in 'roméite' from Fianel, Switzerland; Brugger *et al*., 1997), and the assignment of Fe does not significantly affect the cation distribution.

On the contrary, the variety with the discredited name 'lewisite', from Tripuhy, Minas Gerais, Brazil (Hussak and Prior, 1895) shows a large Fe content (e.g. Fe_2O_3 3.8 wt.%; Rouse *et al*., 1998). This iron was considered as Fe^{3+} and assigned to the *B* site by Rouse *et al*. (1998), whereas Zubkova *et al*. (2000) placed Fe^{3+} at the *A* site. Actually, if iron is assumed as trivalent, it should be hosted at the *B* site, in agreement with Rouse *et al*. (1998) who also reported the IR spectrum for 'lewisite', demonstrating the occurrence of structural OH^{-} groups.

The replacement of Sb^{5+} by Fe^{3+} at the *B* site requires additional substitutions. We can hypothesize two possible mechanism: (1) $^{B}Sb^{5+} + 2^{A}Me^{2+} \leftrightarrow {}^{B}Fe^{3+} + 2^{A}Sb^{3+}$; and (2) $^{B}Sb^{5+} + 2^{Y}O^{2-} \leftrightarrow {}^{B}Fe^{3+} + 2^{Y}(OH,F)^{-}$ where Me^{2+} is usually Ca^{2+}. In hydroxycalcioroméite the second mechanism could play an important role, owing to the

presence of hydroxyl groups. The specimen from the Buca della Vena mine has a very large iron content, 5.52 wt.%, and consequently the correct assignment of iron to the *A* and/or the *B* sites can be a critical factor in calculating a reliable Sb_2O_5:Sb_2O_3 ratio. Unfortunately, owing to the small size and the scarcity of available material, ^{57}Fe Mössbauer spectroscopy could not be performed. Consequently, we tested two possible endmember situations: in the first case, Fe was assumed to be Fe^{3+}, in the second one, Fe^{2+}.

If Fe is assumed as Fe^{3+}, the total sum of the chemical analysis would be 101.39 wt.%. The Fe^{3+} would have to be hosted at the *B* site, and consequently the two possible substitution mechanisms reported above can be discussed. The substitution (1) would lead to an important increase of the mean electron density at the *A* site, owing to a significant amount of Sb^{3+} necessary to balance the substitution of Sb^{5+} by Fe^{3+}. This result disagrees with the mean electron density obtained through the X-ray single-crystal study. On the other hand, the substitution (2) can be discarded, because IR and micro-Raman spectroscopies indicated that no OH^- groups were present in the material studied, and consequently only a fraction of Fe can be hosted at the *B* site, with fluorine substituting for oxygen atoms at the *Y* site.

If Fe is assumed to be Fe^{2+}, a simple homovalent substitution $Ca^{2+} \leftrightarrow Fe^{2+}$ can occur at the *A* site. The occurrence of iron at the *A* site agrees with the observed site scattering at the two cation sites and does not require additional substitutions.

Sb^{5+}:Sb^{3+} ratio

As stated above, the substitution (1) involving Sb^{5+} and Fe^{3+} is not supported by the crystal-structure refinement. Consequently, the Sb^{5+}:Sb^{3+} atomic ratio can be calculated taking into account the substitution of Sb^{5+} by Ti^{4+} and by very minor amounts of Al^{3+}, V^{3+}, and probably Sn^{4+} (as discussed previously, Sn could also be hosted at the *A* site as Sn^{2+}).

There are several possible mechanisms. Two are reported above (1 and 2), with Fe^{3+} replaced by Me^{3+}, where Me = Al, V. Two other possible substitutions are: (3) $^{A}Ca^{2+} + {}^{B}Sb^{5+} \leftrightarrow {}^{A}Sb^{3+} + {}^{B}Me^{4+}$, and (4) $^{B}Sb^{5+} + {}^{Y}O^{2-} \leftrightarrow {}^{B}Me^{4+} + {}^{Y}F^{-}$, where Me = Ti, Sn. In the specimen studied, the occurrence of Sb^{3+} at the *A* site is in agreement with substitution 3).

Ca^{2+} – Na^{+} substitution

The introduction of Na^+ replacing Ca^{2+} at the *A* site requires some heterovalent substitutions. Three possible mechanisms can be hypothesized: (5) $^{A}Ca^{2+} + {}^{A}\square \leftrightarrow 2{}^{A}Na^{+}$; (6) $^{A}Ca^{2+} + {}^{Y}O^{2-} \leftrightarrow {}^{A}Na^{+} + {}^{Y}F^{-}$; and (7) $2{}^{A}Ca^{2+} \leftrightarrow {}^{A}Na^{+} + {}^{A}Sb^{3+}$.

Due to the small amount of sodium and fluorine in oxycalcioroméite, we are not able to understand which mechanism is involved in the replacement of calcium by sodium.

In the roméite group, the existence of members with Na as the dominant cation of the dominant valence at the *A* site is problematic; in fact, the pure terms $Na_2Sb_2^{5+}O_6O$ and $Na_2Sb_2^{5+}O_6(OH,F)$ are not charge balanced, with an excess of two and one negative charges, respectively. Consequently, Na has to be partially replaced by higher-charged cations, like Ca^{2+} or Sb^{3+}, e.g. $(NaCa)_{\Sigma=2}Sb_2^{5+}O_6(OH,F)$ or $(Na_{1.5}Sb_{0.5}^{3+})_{\Sigma=2}Sb_2^{5+}O_6(OH,F)$. Actually, Matsubara *et al*. (1996) described a mineral corresponding to 'fluornatroroméite' with the ideal chemical formula $(NaCa)_{\Sigma=2}Sb_2^{5+}O_6F$.

Discussion

As shown in the previous paragraphs, the chemical composition of oxycalcioroméite deviates from ideality owing to a series of homo- and heterovalent substitutions.

Taking into account the site-scattering values, our single-crystal X-ray study supports the hypothesis that iron occurs predominantly as Fe^{2+} at the *A* site. We cannot exclude the presence of minor amounts of Fe^{3+} at the *B* site, but the atomic ratio Fe^{2+}:Fe^{3+} cannot be determined. According to some authors (e.g. Christy and Gatedal, 2005), the occurrence of Fe^{2+} and Sb^{5+} in the same compound is problematic. On the contrary, taking into account the redox potentials, and in agreement with Mellini *et al*. (1983), the Fe^{2+}/Sb^{5+} pair is favoured over the Fe^{3+}/Sb^{3+} pair. Owing to the fact that tripuhyite, originally described as $Fe_2^{2+}Sb_2^{5+}O_7$ (Hussak and Prior, 1897), has been redefined as $Fe^{3+}Sb^{5+}O_4$ (Berlepsch *et al*., 2003), oxycalcioroméite could be the first example of the combination Fe^{2+}/Sb^{5+}.

The Sb_2O_5:Sb_2O_3 ratio was calculated using two assumptions: (1) all iron was assumed as Fe^{2+}, hosted at the *A* site, and (2) the replacement of Sb^{5+} by tetra- and trivalent cations at the *B* site was balanced through the introduction of Sb^{3+} at the *A* site. It may be an oversimplification, but the

TABLE 7. Bond-valence calculations for oxycalcioroméite, in valence units (vu), according to Brese and O'Keeffe (1991) and Mills *et al*. (2009).

Site	O1	O2	Σ cations	Theoretical
A	$^{6\times}0.12^{\times 2}$	$^{2\times}0.33^{7\times 4}$	1.38	1.49
A′	0.12 $^{2\times}0.06$	$0.08^{\times 2}$ $0.07^{\times 2}$	0.39	0.50
B	$^{6\times}0.81^{\times 2}$		4.86	4.84
Σ anions	2.04	1.62		
Theor.	2.00	1.64		

Left and right superscripts indicates the number of bonds involving cations and anions, respectively.

proposed site occupancies, based on these two assumptions, agree with the refined site-scattering (see the 'Crystal-structure description' section). The bond-valence balance, given in Table 7 and calculated according to Brese and O'Keeffe (1991) and Mills *et al*. (2009), is in satisfying agreement with the expected values.

Acknowledgements

Electron microprobe analyses were performed with the assistance of Raul Carampin. The authors are grateful to the mineral collectors Luigi Pierotti and Ugo Quilici for providing us with the samples of oxycalcioroméite. Marcello Mellini is thanked for the useful discussion about the oxidation state of iron and antimony. The authors are also grateful to Monica Favaro for her scientific and technical help with the IR spectroscopy. Comments by Eugeny V. Gałuskin and an anonymous reviewer helped to improve the paper.

References

Andrade, M.B., Atencio, D., Chukanov, N.V. and Ellena, J. (2013) Hydrokenomicrolite, $(\square,H_2O)_2Ta_2(O,OH)_6(H_2O)$, a new microlite group mineral from Volta Grande pegmatite, Nazareno, Minas Gerais, Brazil. *American Mineralogist*, **98**, 292–296.

Andrade, M.B., Atencio, D., Yang, H., Downs, R.T., Persiano, A.I.C. and Ellena, J. (2012) Fluorcalciomicrolite, IMA 2012-036. CNMNC Newsletter No. 14, October 2012, page 1286: *Mineralogical Magazine*, **76**, 1281–1288.

Atencio, D., Andrade, M.B., Christy, A.G., Gieré, R. and Kartashov, P.M. (2010) The pyrochlore supergroup of minerals: nomenclature. *The Canadian Mineralogist*, **48**, 673–698.

Atencio, D., Ciriotti, M.E. and Andrade, D. (2013) Fluorcalcioroméite, $(Ca,Na)_2Sb_2^{5+}(O,OH)_6F$, a new roméite-group mineral from Starlera mine, Ferrera, Grischun, Switzerland: description and crystal structure. *Mineralogical Magazine*, **77**, 467–473.

Bahfenne, S. and Frost, R.L. (2009) Vibrational spectroscopic study of the antimonate mineral bindheimite $Pb_2Sb_2O_6(O,OH)$. *Spectrochimica Acta*, **A74**, 100–103.

Bahfenne, S. and Frost, R.L. (2010) Raman spectroscopic study of the antimonite mineral roméite. *Spectrochimica Acta*, **A75**, 637–639.

Benvenuti, M., Lattanzi, P., Tanelli, G. and Cortecci, G. (1986) The Ba-Fe-pyrite deposit of Buca della Vena, Apuan Alps, Italy. *Rendiconti della Società Italiana di Mineralogia e Petrologia*, **41**, 347–358.

Berlepsch, P., Armbruster, T., Brugger, J., Criddle, A.J. and Graeser, S. (2003) Tripuhyite, $FeSbO_4$, revisited. *Mineralogical Magazine*, **67**, 31–46.

Biagioni, C. (2009) *Minerali della Provincia di Lucca*. Associazione Micro-mineralogica Italiana, Cremona, Italy, 352 pp.

Bindi, L., Zoppi, M. and Bonazzi, P. (2006) Plumbomicrolite from the Ploskaya Mountain, Keivy Massif, Kola Peninsula, Russia: composition and crystal structure. *Periodico di Mineralogia*, **75**, 51–58.

Brese, N.E. and O'Keeffe, M. (1991) Bond-valence parameters for solids. *Acta Crystallographica*, **B47**, 192–197.

Brugger, J., Gieré, R., Graeser, S. and Meisser, N. (1997) The crystal chemistry of roméite. *Contributions to Mineralogy and Petrology*, **127**, 136–146.

Bruker AXS Inc. (2004) APEX 2. Bruker Advanced X-ray Solutions, Madison, Wisconsin, USA.

Carmignani, L., Dessau, G. and Duchi, G. (1976) I giacimenti a barite, pirite e ossidi di ferro delle Alpi Apuane. Studio minerogenetico e strutturale. Nuove osservazioni sui giacimenti polimetallici. *Bollettino della Società Geologica Italiana*, **95**, 1009–1061.

Černý, P., Hawthorne, F.C., Laflamme, J.H.G. and Hinthorne, J.R. (1979) Stibiobetafite, a new member of the pyrochlore group from Vežná, Czechoslovakia. *The Canadian Mineralogist*, **17**, 583–588.

Christy, A.G. and Atencio, D. (2013) Clarification of status of species in the pyrochlore supergroup. *Mineralogical Magazine*, **77**, 13–20.

Christy, A.G. and Gatedal, K. (2005) Extremely Pb-rich rock-forming silicates including a beryllian scapolite and associated minerals in a skarn from Långban, Värmland, Sweden. *Mineralogical Magazine*, **69**, 995–1018.

Chukanov, N.V., Blass, G., Zubkova, N.V., Pekov, I.V., Pushcharovskii, D.Yu. and Prinz, H. (2013) Hydroxymanganopyrochlore: a new mineral from the Eifel Volcanic Region, Germany. *Transactions (Doklady) of the Russian Academy of Sciences/Earth Science Section*, **449**, 342–345.

Cortecci, G., Lattanzi, P. and Tanelli, G. (1985) Barite-iron oxide-pyrite deposits from Apuane Alps (Northern Tuscany, Italy). *Memorie della Società Geologica Italiana*, **30**, 337–345.

Ercit, T.S., Černý, P. and Hawthorne, F.C. (1993) Cesstibtantite – a geologic introduction to the inverse pyrochlores. *Mineralogy and Petrology*, **48**, 235–255.

Fellin, M.G., Reiners, P.W., Brandon, M.T., Wüthrich, E., Balestrieri, M.L. and Molli, G. (2007) Thermochronologic evidence for the exhumational history of the Alpi Apuane metamorphic core complex, northern Apennines, Italy. *Tectonics*, **26**, TC6015.

Frost, R.L. and Bahfenne, S. (2010) Raman spectroscopic study of the antimonite mineral lewisite, $(Ca,Fe,Na)_2(Sb,Ti)_2O_6(O,OH)_7$. *Radiation Effects and Defects in Solids*, **165**, 46–53.

Hussak, E. and Prior, G.T. (1895) Lewisite and zirkelite, two new Brazilian minerals. *Mineralogical Magazine*, **11**, 80–88.

Hussak, E. and Prior, G.T. (1897) On tripuhyite, a new antimonate of iron, from Tripuhy, Brazil. *Mineralogical Magazine*, **11**, 302–303.

Holland, T.J.B. and Redfern, S.A.T. (1997) Unit cell refinement from powder diffraction data: the use of regression diagnostics. *Mineralogical Magazine*, **61**, 65–77.

Kraus, W. and Nolze, G. (1996) POWDER CELL – a program for the representation and manipulation of crystal structures and calculation of the resulting X-ray powder patterns. *Journal of Applied Crystallography*, **29**, 301–303.

Mandarino, J.A. (1979) The Gladstone-Dale relationship. Part III: some general applications. *The Canadian Mineralogist*, **17**, 71–76.

Mandarino, J.A. (1981) The Gladstone-Dale relationship. Part IV. The compatibility concept and its application. *The Canadian Mineralogist*, **19**, 441–450.

Matsubara, S., Kato, A., Shimizu, M., Sekiuchi, K. and Suzuki, Y. (1996) Romeite from Gozaisho mine, Iwaki, Japan. *Mineralogical Journal*, **18**, 155–160.

Mellini, M., Orlandi, P. and Perchiazzi, N. (1983) Derbylite from Buca della Vena mine, Apuan Alps, Italy. *The Canadian Mineralogist*, **21**, 513–516.

Mills, S.J., Christy, A.G., Chen, E.C-C. and Raudsepp, M. (2009) Revised values of the bond valence parameters for $^{[6]}Sb(V)-O$ and $^{[3,11]}Sb(III)-O$. *Zeitschrift für Kristallographie*, **224**, 423–431.

Orberger, B. (1985) *Les gisements de barytine – pyrite – oxydes de fer de la région de Santa Anna (Alpes Apuanes, Toscane, Italie)*. Thesis, University of Nancy, France, 263 pp.

Orlandi, P. and Dini, A. (2004) Die mineralien der Buca della Vena mine, Apuaner Berge, Toskana, Italien. *Lapis*, **1/2004**, 11–24.

Rouse, R.C., Dunn, P.J., Peacor, D.R. and Wang, L. (1998) Structural studies of the natural antimonian pyrochlores. I. Mixed valency, cation site splitting, and symmetry reduction in lewisite. *Journal of Solid State Chemistry*, **141**, 562–569.

Shannon, R.D. (1976) Revised effective ionic radii and systematic studies of interatomic distances in halides and chalcogenides. *Acta Crystallographica*, **A32**, 751–767.

Sheldrick, G.M. (2008) A short history of SHELX. *Acta Crystallographica*, **A64**, 112–122.

Wilson, A.J.C. (1992) *International Tables for X-ray Crystallography*, Volume C. Kluwer, Dordrecht, The Netherlands.

Witzke, T., Steins, M., Doering, T., Schuckmann, W., Wegner, R. and Pöllmann, H. (2011) Fluornatromicrolite, $(Na,Ca,Bi)_2Ta_2O_6F$, a new mineral from Quixaba, Paraíba, Brazil. *The Canadian Mineralogist*, **49**, 1105–1110.

Zubkova, N.V., Pushcharovksy, D.Yu., Atencio, D., Arakcheeva, A.V. and Matioli, P.A. (2000) The crystal structure of lewisite, $(Ca,Sb^{3+},Fe^{3+},Al,Na,Mn,\square)_2(Sb^{5+},Ti)_2O_6(OH)$. *Journal of Alloys and Compounds*, **296**, 75–79.